

Resonant Versus Nonresonant Spin Readout of a Nitrogen-Vacancy Center in Diamond under Cryogenic Conditions

Richard Monge^{1,2,*}, Tom Delord^{1,*}, Gergő Thiering³, Ádám Gali^{3,4} and Carlos A. Meriles^{1,2,†}

¹*Department of Physics, CUNY-City College of New York, New York, New York 10031, USA*

²*CUNY-Graduate Center, New York, New York 10016, USA*

³*HUN-REN Wigner Research Centre for Physics, P.O. Box 49, H-1525 Budapest, Hungary*

⁴*Department of Atomic Physics, Institute of Physics, Budapest University of Technology and Economics, Műegyetem rakpart 3., H-1111 Budapest, Hungary*



(Received 11 July 2023; accepted 23 October 2023; published 5 December 2023)

The last decade has seen an explosive growth in the use of color centers for metrology applications, the paradigm example arguably being the nitrogen-vacancy (NV) center in diamond. Here, we focus on the regime of cryogenic temperatures and examine the impact of spin-selective, narrow-band laser excitation on NV readout. Specifically, we demonstrate a more than fourfold improvement in sensitivity compared to that possible with nonresonant (green) illumination, largely due to a boost in readout contrast and integrated photon count. We also leverage nuclear spin relaxation under resonant excitation to polarize the ^{14}N host, which we then prove beneficial for spin magnetometry. These results open opportunities in the application of NV sensing to the investigation of condensed matter systems, particularly those exhibiting superconducting, magnetic, or topological phases selectively present at low temperatures.

DOI: [10.1103/PhysRevLett.131.236901](https://doi.org/10.1103/PhysRevLett.131.236901)

The ability to initialize and read out the spin state of individual magneto-optically active color centers is presently driving extensive work aimed at their use as local probes to sense temperature, pressure, or electric and magnetic fields with spatial resolution down to the nanoscale [1]. Among a rapidly growing palette of material systems—including, e.g., color centers in silicon carbide [2,3] and hexagonal boron nitride [4,5]—the nitrogen-vacancy (NV) center in diamond stands out as a leading sensing platform due to a favorable combination of fluorescence brightness, readout contrast, and spin coherence lifetime.

While ambient operation has been key to their success, bringing NVs to cryogenic conditions creates opportunities for control schemes not possible at room temperature. Indeed, orbital averaging of the NV first excited manifold—fast at 300 K—effectively vanishes below ~ 20 K [6,7] leading to a set of narrow, spin selective optical transitions, already exploited, e.g., in demonstrations of spin-photon [8] and photon-mediated, interspin entanglement [9]. NV sensing protocols adapted to the cryogenic regime are less developed but equally attractive, particularly given the growing number of studies centered on condensed matter phases selectively present at low temperatures [10–14]. For example, recent work used resonantly tuned laser light between the ground and first excited NV manifolds at ~ 4 K to attain single-shot readout fidelity through efficient spin-to-charge conversion without resorting to high magnetic fields or photon-collection optics [15,16].

Despite their superior fidelity, spin-to-charge methods are not necessarily optimal because their intrinsically longer readout times—typically a few milliseconds—carry a concomitant overhead, countered only in sensing protocols demanding extended evolution intervals (such as, e.g., spin-lattice relaxation measurements [17–19]). On the other hand, standard (i.e., nonresonant) optical readout schemes tend to work more poorly at lower temperatures because electric-field and strain-induced excited state anticrossings—affecting individual NVs differently—are often detrimental to spin initialization and readout [20].

Here, we investigate NV spin readout under resonant laser light in the regime of low temperatures and low magnetic fields. We first characterize the NV spin dynamics in the presence of tunable, narrow-band optical excitation, and make use of spin initialization and readout schemes with minimal overhead to attain a multifold detection sensitivity boost (typically ~ 4 times, depending on the chosen NV) compared to nonresonant methods. We then turn our attention to the interplay between the NV and the ^{14}N host, and show that resonant illumination alters the electronic and nuclear spin states on comparable timescales. We capitalize on this finding to polarize the ^{14}N spin without resorting to radio-frequency (rf) pulses, which we subsequently show to be advantageous for applications to magnetic sensing.

Optical spectroscopy at cryogenic temperatures.—Throughout our experiments, we investigate naturally occurring NV centers in a [100] electronic grade diamond using a homemade, multicolor confocal microscope based on a close-cycle cryo-workstation [21,22]. The system

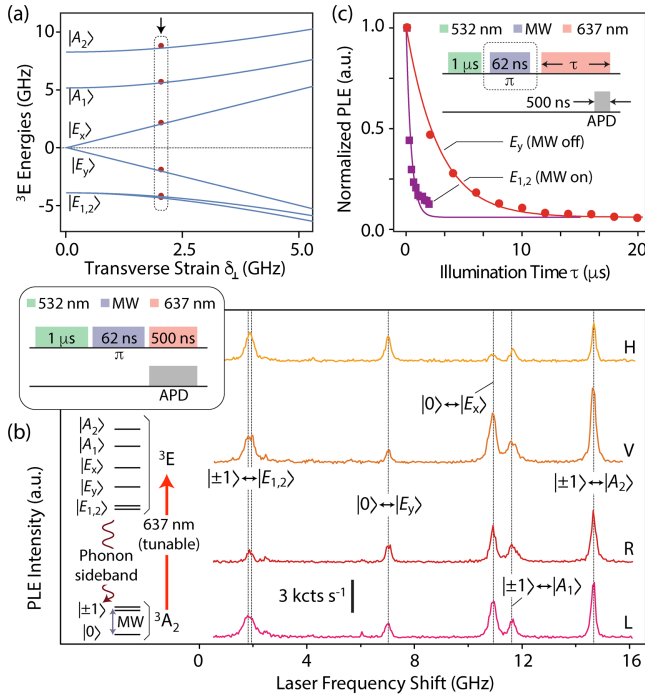


FIG. 1. Resonant spectroscopy of NV centers. (a) 3E energy diagram as a function of transverse strain. (b) PLE spectroscopy of a representative single NV; peak positions are signaled in (a) by the boxed dots. *V* and *H* indicate linear polarization of the probe beam along perpendicular planes; *L* and *R* denote opposite circular polarization helicity. The MW π -pulse makes $m_S = \pm 1$ transitions visible (even if the amplitude of the $m_S = 0$ resonances is less than optimal). Frequencies are relative to 470.488 THz; spectra have been vertically offset for clarity. (c) PLE amplitude as a function of the red illumination duration under an *L*-polarized beam for the E_y and $E_{1,2}$ transitions; solid lines are exponential fits with time constants 3.11 ± 0.08 and 0.19 ± 0.02 μ s, respectively. The green (red) laser power is 500 μ W (4 μ W), and the MW frequency—resonant with the ground state $|0\rangle \leftrightarrow | - 1\rangle$ transition—is 2.809 GHz; the temperature is 5 K and we apply a weak magnetic field of 0.2 mT.

features green and red laser light sources (respectively, 532 and 637 nm); the latter is narrow-band (500 kHz) and tunable over a 4 nm range. We use half- and quarter-wave plates to control both the red beam plane of polarization and helicity, and collect the Stokes-shifted NV fluorescence using a 650-nm high-pass filter and a single-photon avalanche photodetector (APD). We attain ground state control of the NV spin through the microwave (MW) field produced by an antenna in the form of a thin copper wire overlaid on the diamond surface.

Figure 1(a) lays out the calculated NV 3E excited state manifold [22–33]: As an orbital doublet and spin triplet, it features six different states whose relative alignment and degeneracy depend on local strain and electric field. In our experiments, we tune the red laser to induce transitions between the 3E and the ground state, 3A_2 , also a spin triplet but an orbital singlet whose response to local fields is

weaker and has been ignored. Figure 1(b) shows example photo-luminescence excitation (PLE) spectra for a low-strain ($\delta_{\perp} \approx 3$ GHz) bulk NV under variable laser light polarization [22]. Except for $|E_x\rangle$ and $|E_y\rangle$ —primarily associated to the $m_S = 0$ spin projection—most eigenstates in the 3E manifold are entangled states of spin and orbital angular momentum [34]. Correspondingly, resonant optical excitation produces a transition-dependent decline of the observed fluorescence due to gradual spin depletion [35]; the decay rate is substantially smaller for the $|E_x\rangle$ and $|E_y\rangle$ resonances, which we hence refer to hereafter as the “cycling” transitions [Fig. 1(c)].

NV readout under optically selective excitation.—A key metric for applications of single spin-active color centers to sensing is given by the sensitivity η , expressed herein as

$$\eta = \frac{\mathcal{A}}{\sqrt{N}t_E} e^{-\frac{t_E}{t_C}} \sqrt{\left(1 + \frac{1}{\mathcal{C}^2 n_{\text{avg}}}\right) \left(\frac{t_I + t_R + t_E}{t_E}\right)}, \quad (1)$$

where \mathcal{C} is the effective spin contrast, n_{avg} is the net number of photons during the readout time t_R , t_E denotes the “evolution” (i.e., spin-signal-encoding) time, t_I is the system initialization time, and t_C is a sequence-specific NV spin coherence lifetime; N represents the total number of repeats, and \mathcal{A} is a constant that depends on the specific transduction mechanism connecting the color center spin to the external stimulus being measured (e.g., electric, magnetic, etc.).

Resonant NV spin readout is particularly favorable at a cycling transition because both the contrast and integrated photon counts are greater compared to those possible under standard green illumination. As a first illustration, Fig. 2(a) shows pulsed optically detected magnetic resonance (ODMR) data at 7 K for the NV in Fig. 1 using green and red (E_y) readouts; the protocol uses a green laser pulse to initialize the NV charge [36] (preferentially into negative) and spin [37] states (predominantly into $m_S = 0$). A clear readout sensitivity gain—approximately 4.3 times in this case—emerges under resonant excitation, largely a consequence of the greater integrated photon count (n_{avg} is 8.8×10^{-2} per readout for red light but only 5.9×10^{-3} for green [22]). Further, the readout contrast \mathcal{C} —weaker in a pulsed ODMR experiment due to MW spectral selectivity—also experiences a boost under resonant illumination reaching up to 78%, limited by NV spin initialization [15,16] [Fig. 2(b)]. The result is an enhanced detection sensitivity even in a routine sensing protocol like this one, with comparable—if not better—improvements expected in all other (more time-consuming) NV control schemes. Figure 2(c) displays an example in the form of NV Rabi responses using resonant and nonresonant readout; the signal-to-noise ratio (SNR) boost is substantial, here exposed upon imposing a common experimental time of 120 s. We have observed comparable—if slightly

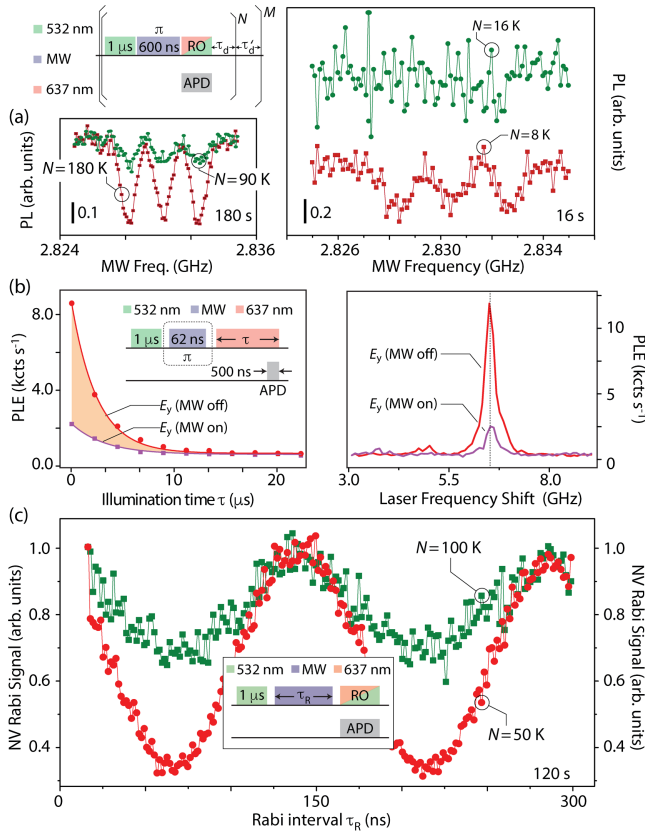


FIG. 2. Comparison of NV resonant and nonresonant readout. (a) (Top left) Pulsed ODMR using red (637 nm) or green (532 nm) readout (RO); τ_d and τ'_d are hardware-imposed delays. (Right) ODMR for the NV in Fig. 1 using green or red readout (upper and lower traces, respectively); in both cases, the number of sampled frequencies is $M = 101$ and the experimental time is 16 s (Bottom left) Same as before but for an experimental time of 180 s. (b) (Left) PLE amplitude for the E_y transition with or without MW inversion; resonant readout results from the integrated photon count difference (shaded area). (Right) E_y photoluminescence as a function of laser frequency using the protocol in the left plot but with a fixed red illumination time (0.5 μ s). (c) NV spin Rabi signal for resonant and non-resonant readout (red circles and green squares, respectively) as a function of the MW pulse duration for a common 120 s experiment time; in (a) and (c), the red (green) readout time is 5 μ s (0.3 μ s). In all these experiments, the red (green) laser power is 10 μ W (500 μ W) and the magnetic field— $\sim 5^\circ$ misaligned with the NV axis—is ~ 2 mT.

smaller—sensitivity gains for other NVs throughout the crystal [22].

Polarization of the nuclear spin host.—An open question relevant to NV cryosensing applications is the impact of selective optical excitation on the nuclear spin polarization of the nitrogen host. Specifically, we are interested in determining the timescale over which resonant illumination alters the starting nuclear spin state. We address this problem in Fig. 3, where we first initialize the NV spin into $|m_S = -1\rangle$ using a population trapping protocol

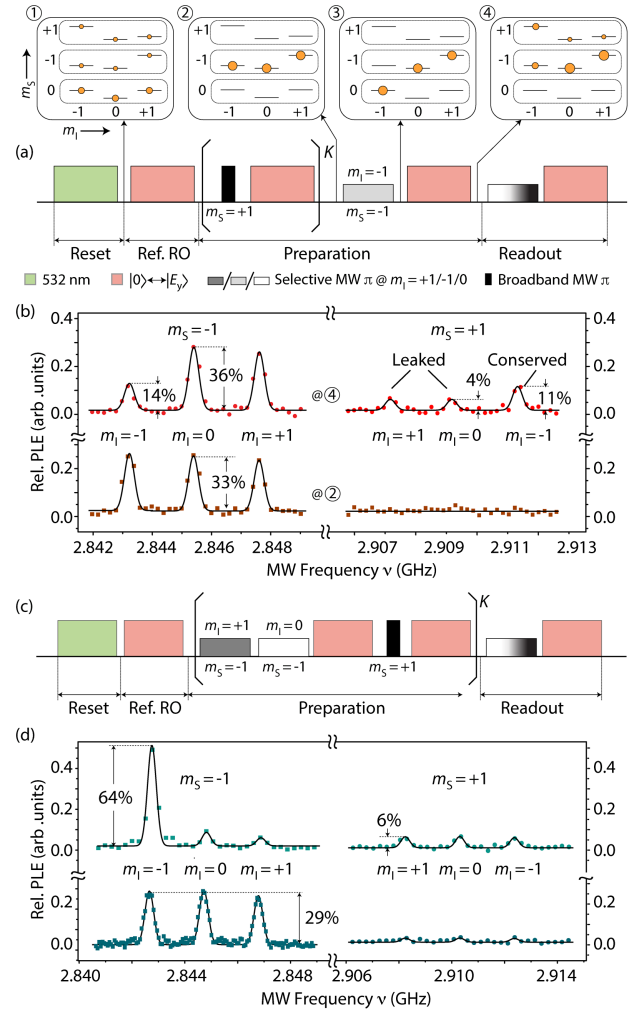


FIG. 3. rf-free spin polarization of the ^{14}N host. (a) To study the action of resonant excitation on the ^{14}N nuclear spin state, we first initialize the electronic spin state into $m_S = -1$ manifold. Upon selective MW inversion of the $|m_S = -1, m_I = +1\rangle$ state and resonant excitation of the $|E_y\rangle$ transition, we probe the hyperfine populations in the $m_S = +1$ manifold. (b) NV ODMR spectrum after application of the protocol in (a) using $K = 5$; the lower dataset shows the background signal obtained in the absence of a selective π pulse in the $m_S = -1$ manifold. (c) ^{14}N nuclear spin polarization protocol. (d) NV ODMR spectrum upon application of the protocol in (c) for $K = 6$; the lower traces are the spectra in the absence of selective $m_S = -1$ pulses. In (a) and (c), we use a color gradient to denote a selective MW π pulse whose frequency we vary for spectrum reconstruction. In (b) and (d), percent values indicate the estimated fractional nuclear spin populations with errors within $\pm 2\%$; solid lines are Gaussian fits. The red (green) laser power is 1 μ W (100 μ W) and the MW pulses are 2.4 μ s long. Ref. RO: Reference readout.

comprising sequential optical excitation and electronic spin state inversion [15]. Upon selectively populating one of the hyperfine levels in the $|m_S = 0\rangle$ manifold (specifically, the $|m_S = 0, m_I = -1\rangle$ state in Fig. 3), we determine the optically induced change in the nuclear spin state by

reconstructing the NV ODMR spectrum following resonant optical spin depletion of $|m_S = 0\rangle$ [see schematics in Fig. 3(a)].

Figure 3(b) shows the results: Comparison of the relative hyperfine peak amplitudes—correlating with the nuclear spin populations after resonant optical excitation—shows that a single cycle of electronic spin depletion has a significant probability (approximately 30%) to simultaneously flip the nuclear spin state, even in the case of a cycling transition such as the $|m_S = 0\rangle \leftrightarrow |E_y\rangle$ probed here. While hyperfine states are known to be fragile against green optical excitation at low magnetic fields [38], the above result is surprising in that the $|E_y\rangle$ state has a predominant $m_S = 0$ character [34], and hence one would naively anticipate a reduced hyperfine coupling or, equivalently, a slow nuclear spin flip rate. Further, we find that starting from $|m_I = -1\rangle$, both $|m_I = 0\rangle$ and $|m_I = +1\rangle$ populate comparably under resonant illumination, thus pointing to efficient double-quantum nuclear spin relaxation processes. A detailed analysis suggests single- and double-quantum flips stem from complementary channels, associated with transverse hyperfine and quadrupolar couplings, respectively [22].

While a fuller understanding of the dynamics at play will require additional work, one important implication for NV sensing is that one can combine resonant illumination and selective MW excitation to polarize the nuclear spin state of the nitrogen host without resorting to radio-frequency pulses [39]. We illustrate this notion in Figs. 3(c) and 3(d) where we modify the protocol in Fig. 3(a) to trap the NV population into the $|m_S = -1, m_I = -1\rangle$ state prior to optical spin readout. From an analysis of the resulting ODMR spectrum, we conclude the spin trapping efficiency here reaches up to 64%, limited by imperfect spin depletion of the $m_S = 0$ manifold [22].

Interestingly, the above nuclear spin polarization scheme is not unique as other, less time-consuming routes are also possible, though at the expense of a reduced polarization efficiency. To illustrate this point, we return to the regular ODMR protocol in Fig. 2(a), though this time we extend the duration of the MW pulses (2.4 μ s) to attain good spectral resolution [red trace in the upper plot of Fig. 4(a)]. Remarkably, we find that the contrast we attain via selective MW excitation (reaching up to 39%) exceeds that possible for an NV center whose nuclear spin host is unpolarized ($\sim 23\%$), as we confirm by comparing to the ODMR signal under 80-ns-long π pulses [featuring $\sim 70\%$ contrast, see brown trace in the lower plot of Fig. 4(a)]. An in-depth analysis [22] shows this response stems from a measurement-induced process during the ODMR sequence, where multiple repeats of resonant optical and MW excitation combine to preferentially populate the hyperfine state under observation. Note that the contrast we attain under selective MW excitation [smaller than in Fig. 3(d) but greater than the best possible under green readout, see faint green trace in the lower plot of Fig. 4(a)] depends delicately on the

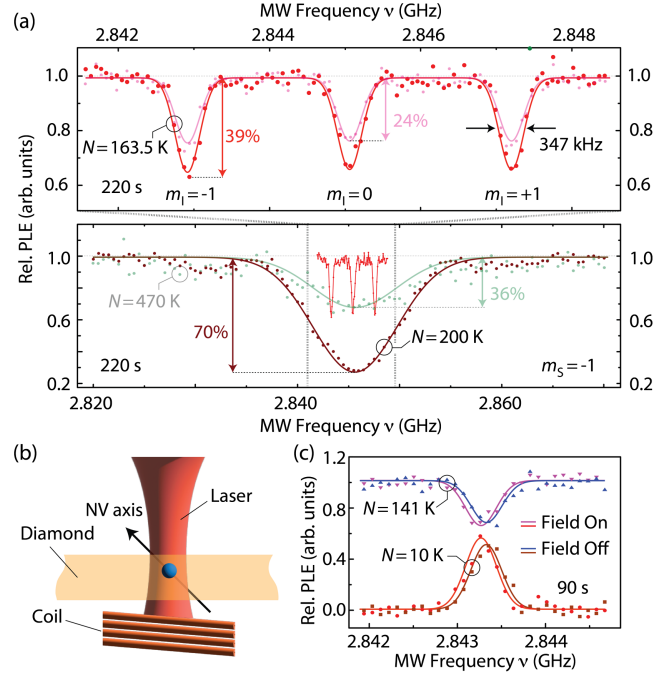


FIG. 4. Magnetometry with nuclear-spin-polarized NVs. (a) (Bottom plot) NV ODMR spectroscopy using the protocol of Fig. 2(a) using a 5- μ s red readout and selective (2.4 μ s) or broadband (89 ns) π pulses (red and brown traces, respectively). For reference, the faint green trace in the back shows the NV ODMR spectrum under standard green readout (300 ns). In all cases, the number of sampled frequencies is $M = 101$, the experimental duration is 220 s, and the green initialization pulse is 2 μ s. (Upper plot) Zoomed NV ODMR spectrum under selective MW excitation. The faint pink trace shows the same result but for 5- μ s-long green initialization pulses, resulting in reduced contrast. (b) Schematics of the experimental setup. (c) NV ODMR spectra with or without a coil-generated, ~ 3 μ T magnetic field. The upper traces use the conditions in Fig. 4(a) (red set) to induce partial nuclear spin polarization; in the lower traces, we apply the protocol in Fig. 3(c). In (a) and (c), solid lines are Gaussian fits.

duration of the 532-nm initialization pulse, consistent with the scrambling action of green illumination on the nuclear spin [29] [see faint pink trace in the upper plot of Fig. 4(a)].

Magnetometry with a spin-polarized host.—The ability to initialize the nuclear spin host translates into a higher sensitivity to magnetic field shifts. We experimentally demonstrate this notion in Fig. 4(b) where we use a small coil adjacent to the diamond crystal to controllably change the external magnetic field by a small amount. Interestingly, the “direct current” (dc) magnetic sensitivity we attain via a measurement-induced ^{14}N polarization [$\eta_{\text{DC}}^{(\text{MI})} = 1.74 \pm 0.50$ $\mu\text{T Hz}^{-1/2}$, upper traces in Fig. 4(c)] is comparable to that resulting from resorting to the active nuclear polarization protocol of Fig. 3(c) [$\eta_{\text{DC}}^{(\text{AP})} = 0.90 \pm 0.12$ $\mu\text{T Hz}^{-1/2}$, lower traces in Fig. 4(c)], largely due to a much reduced overhead. Comparing to the sensitivity

possible in our setup via green readout, the results above correspond to six- or sevenfold enhancements for this NV; we find comparable improvements for others, and expect as high as tenfold boosts for longer NV coherence [22].

In summary, we have shown how resonant optical excitation under cryogenic conditions can improve NV spin detection sensitivity over standard green readout. At the low magnetic fields present in our experiments, 637-nm light induces unexpectedly fast nuclear spin flips of the nitrogen host, a finding we exploited to demonstrate efficient ^{14}N polarization. Combining resonant excitation and nuclear spin initialization, we demonstrated improved dc magnetic field sensitivity. Note that ^{14}N spin polarization should also have a positive impact on the attainable sensitivity to “alternating current” (ac) magnetic fields, not only due to the greater contrast but also because the narrower spectral bandwidth makes spin decoupling protocols less sensitive to frequency offset. Future work must address the transition from bulk to shallow NVs as surface proximity is known to be detrimental to the cyclicity and brightness of the optical transitions (although the reasons are only partly understood). This effort should prove valuable in the growing set of applications of NV sensing to solid state phases selectively present at low temperatures.

All authors acknowledge support from the National Science Foundation through Grants No. NSF-2216838, No. NSF-2203904, and No. NSF-1914945; R. M. acknowledges support from NSF-2316693. A. G. acknowledges the support from the National Research, Development and Innovation Office of Hungary (NKFIH) in Hungary for the National Excellence Program (Grant No. KKP129866), the Quantum Information National Laboratory (Grant No. 2022-2.1.1-NL-2022-0000), and the EU QuantERA II MAESTRO project; he also acknowledges support from the European Commission through the QuMicro project (Grant No. 101046911). A. G. and G. T. acknowledge the high-performance computational resources provided by the Governmental Agency for IT Development Institute of Hungary (KIFÜ). All authors also acknowledge access to the facilities and research infrastructure of the NSF CREST IDEALS, Grant No. NSF-2112550.

*These authors contributed equally to this work.

†Corresponding author: cmeriles@ccny.cuny.edu

- [1] C. L. Degen, F. Reinhard, and P. Cappellaro, Quantum sensing, *Rev. Mod. Phys.* **89**, 035002 (2017).
- [2] W. F. Koehl, B. B. Buckley, F. J. Heremans, G. Calusine, and D. D. Awschalom, Room temperature coherent control of defect spin qubits in silicon carbide, *Nature (London)* **479**, 84 (2011).
- [3] D. Riedel, F. Fuchs, H. Kraus, S. V ath, A. Sperlich, V. Dyakonov, A. A. Soltamova, P. G. Baranov, V. A. Ilyin, and G. V. Astakhov, Resonant addressing and manipulation of

silicon vacancy qubits in silicon carbide, *Phys. Rev. Lett.* **109**, 226402 (2012).

- [4] A. Gottscholl, M. Diez, V. Soltamov, C. Kasper, D. Krau e, A. Sperlich, M. Kianinia, C. Bradac, I. Aharonovich, and V. Dyakonov, Spin defects in hBN as promising temperature, pressure and magnetic field quantum sensors, *Nat. Commun.* **12**, 4480 (2021).
- [5] A. J. Healey, S. C. Scholten, T. Yang, J. A. Scott, G. J. Abrahams, I. O. Robertson, X. F. Hou, Y. F. Guo, S. Rahman, Y. Lu, M. Kianinia, I. Aharonovich, and J.-P. Tetienne, Quantum microscopy with van der Waals heterostructures, *Nat. Phys.* **19**, 87 (2023).
- [6] Kai-Mei C. Fu, C. Santori, P. E. Barclay, L. J. Rogers, N. B. Manson, and R. G. Beausoleil, Observation of the dynamic Jahn-Teller effect in the excited states of nitrogen-vacancy centers in diamond, *Phys. Rev. Lett.* **103**, 256404 (2009).
- [7] A. Batalov, V. Jacques, F. Kaiser, P. Siyushev, P. Neumann, L. J. Rogers, R. L. McMurtrie, N. B. Manson, F. Jelezko, and J. Wrachtrup, Low temperature studies of the excited-state structure of negatively charged nitrogen-vacancy color centers in diamond, *Phys. Rev. Lett.* **102**, 195506 (2009).
- [8] E. Togan, Y. Chu, A. S. Trifonov, L. Jiang, J. Maze, L. Childress, M. V. G. Dutt, A. S. S orensen, P. R. Hemmer, A. S. Zibrov, and M. D. Lukin, Quantum entanglement between an optical photon and a solid-state spin qubit, *Nature (London)* **466**, 730 (2010).
- [9] H. Bernien, B. Hensen, W. Pfaff, G. Koolstra, M. S. Blok, L. Robledo, T. H. Taminiau, M. Markham, D. J. Twitchen, L. Childress, and R. Hanson, Heralded entanglement between solid-state qubits separated by three metres, *Nature (London)* **497**, 86 (2013).
- [10] M. Pelliccione, A. Jenkins, P. Ovarthaiyapong, C. Reetz, E. Emmanouilidou, N. Ni, and A. C. Bleszynski Jayich, Scanned probe imaging of nanoscale magnetism at cryogenic temperatures with a single-spin quantum sensor, *Nat. Nanotechnol.* **11**, 700 (2016).
- [11] L. Thiel, D. Rohner, M. Ganzhorn, P. Appel, E. Neu, B. M uller, R. Kleiner, D. Koelle, and P. Maletinsky, Quantitative nanoscale vortex imaging using a cryogenic quantum magnetometer, *Nat. Nanotechnol.* **11**, 677 (2016).
- [12] S. E. Lillie, D. A. Broadway, N. Dontschuk, S. C. Scholten, B. C. Johnson, S. Wolf, S. Rachel, L. C. L. Hollenberg, and J.-P. Tetienne, Laser modulation of superconductivity in a cryogenic wide-field nitrogen-vacancy microscope, *Nano Lett.* **20**, 1855 (2020).
- [13] L. Thiel, Z. Wang, M. A. Tschudin, D. Rohner, I. Guti errez-Lezama, N. Ubrig, M. Gibertini, E. Giannini, A. F. Morpurgo, and P. Maletinsky, Probing magnetism in 2D materials at the nanoscale with single-spin microscopy, *Science* **364**, 973 (2019).
- [14] T. Song, Q.-C. Sun, E. Anderson, C. Wang, J. Qian, T. Taniguchi, K. Watanabe, M. A. McGuire, R. St ohr, D. Xiao, T. Cao, J. Wrachtrup, and X. Xu, Direct visualization of magnetic domains and Moir e magnetism in twisted 2D magnets, *Science* **374**, 1140 (2021).
- [15] D. M. Irber, F. Poggiali, F. Kong, M. Kieschnick, T. L uhmann, D. Kwiatkowski, J. Meijer, J. Du, F. Shi, and F. Reinhard, Robust all-optical single-shot readout of

- nitrogen-vacancy centers in diamond, *Nat. Commun.* **12**, 532 (2021).
- [16] Q. Zhang, Y. Guo, W. Ji, M. Wang, J. Yin, F. Kong, Y. Lin, C. Yin, F. Shi, Y. Wang, and J. Du, High-fidelity single-shot readout of single electron spin in diamond with spin-to-charge conversion, *Nat. Commun.* **12**, 1529 (2021).
- [17] B. J. Shields, Q. P. Unterreithmeier, N. P. de Leon, H. Park, and M. D. Lukin, Efficient readout of a single spin state in diamond via spin-to-charge conversion, *Phys. Rev. Lett.* **114**, 136402 (2015).
- [18] D. A. Hopper, R. R. Grote, A. L. Exarhos, and L. C. Bassett, Near-infrared-assisted charge control and spin readout of the nitrogen-vacancy center in diamond, *Phys. Rev. B* **94**, 241201(R) (2016).
- [19] H. Jayakumar, S. Dhomkar, J. Henshaw, and C. A. Meriles, Spin readout via spin-to-charge conversion in bulk diamond nitrogen-vacancy ensembles, *Appl. Phys. Lett.* **113**, 122404 (2018).
- [20] J. Happacher, D. A. Broadway, J. Bocquel, P. Reiser, A. Jimenez, M. A. Tschudin, L. Thiel, D. Rohner, Marcel. li Grimau Puigibert, B. Shields, J. R. Maze, V. Jacques, and P. Maletinsky, Low-temperature photophysics of single nitrogen-vacancy centers in diamond, *Phys. Rev. Lett.* **128**, 177401 (2022).
- [21] R. Monge, T. Delord, N. Proscia, Z. Shotan, H. Jayakumar, J. Henshaw, P. Zangara, A. Lozovoi, D. Pagliero, P. D. Esquinazi, T. An, I. Sodemann, V. M. Menon, and C. A. Meriles, Spin dynamics of a solid-state qubit in proximity to a superconductor, *Nano Lett.* **23**, 422 (2023).
- [22] See Supplemental Material <http://link.aps.org/supplemental/10.1103/PhysRevLett.131.236901> for further discussions, which includes Refs. [23–32].
- [23] A. Dréau, M. Lesik, L. Rondin, P. Spinicelli, O. Arcizet, J.-F. Roch, and V. Jacques, Avoiding power broadening in optically detected magnetic resonance of single NV defects for enhanced dc magnetic field sensitivity, *Phys. Rev. B* **84**, 195204 (2011).
- [24] J. F. Barry, J. M. Schloss, E. Bauch, M. J. Turner, C. A. Hart, L. M. Pham, and R. L. Walsworth, Sensitivity optimization for nv-diamond magnetometry, *Rev. Mod. Phys.* **92**, 015004 (2020).
- [25] P. C. Maurer, G. Kucsko, C. Latta, L. Jiang, N. Y. Yao, S. D. Bennett, F. Pastawski, D. Hunger, N. Chisholm, M. Markham, D. J. Twitchen, J. I. Cirac, and M. D. Lukin, Room-temperature quantum bit memory exceeding one second, *Science* **336**, 1283 (2012).
- [26] X. Guo, N. Delegan, J. C. Karsch, Z. Li, T. Liu, R. Shreiner, A. Butcher, D. D. Awschalom, F. J. Heremans, and A. A. High, Tunable and transferable diamond membranes for integrated quantum technologies, *Nano Lett.* **21**, 10392 (2021).
- [27] Y. Chu, N. P. de Leon, B. J. Shields, B. Hausmann, R. Evans, E. Togan, M. J. Burek, M. Markham, A. Stacey, A. S. Zibrov, A. Yacoby, D. J. Twitchen, M. Loncar, H. Park, P. Maletinsky, and M. D. Lukin, Coherent optical transitions in implanted nitrogen vacancy centers, *Nano Lett.* **14**, 1982 (2014).
- [28] M. Kasperczyk, J. A. Zuber, A. Barfuss, J. Kölbl, V. Yurgens, S. Flagan, T. Jakubczyk, B. Shields, R. J. Warburton, and P. Maletinsky, Statistically modeling optical linewidths of nitrogen vacancy centers in microstructures, *Phys. Rev. B* **102**, 075312 (2020).
- [29] L. Orphal-Kobin, K. Unterguggenberger, T. Pregolato, N. Kemf, M. Matalla, R-S. Unger, I. Ostermay, G. Pieplow, and T. Schröder, Optically coherent nitrogen-vacancy defect centers in diamond nanostructures, *Phys. Rev. X* **13**, 011042 (2023).
- [30] A. Gali, M. Fyta, and E. Kaxiras, *Ab initio* supercell calculations on nitrogen-vacancy center in diamond: electronic structure and hyperfine tensors, *Phys. Rev. B* **77**, 155206 (2008).
- [31] I. Bersuker, *The Jahn-Teller Effect* (Cambridge University Press, Cambridge, England, 2006).
- [32] G. Thiering and A. Gali, *Ab initio* calculation of spin-orbit coupling for an NV center in diamond exhibiting dynamic Jahn-Teller effect, *Phys. Rev. B* **96**, 081115(R) (2017).
- [33] M. W. Doherty, N. B. Manson, P. Delaney, and L. C. L. Hollenberg, The negatively charged nitrogen-vacancy centre in diamond: the electronic solution, *New J. Phys.* **13**, 025019 (2011).
- [34] J. R. Maze, A. Gali, E. Togan, Y. Chu, A. Trifonov, E. Kaxiras, and M. D. Lukin, Properties of nitrogen-vacancy centers in diamond: The group theoretic approach, *New J. Phys.* **13**, 025025 (2011).
- [35] Ph. Tamarat, N. B. Manson, J. P. Harrison, R. L. McMurtrie, A. Nizovtsev, C. Santori, R. G. Beausoleil, P. Neumann, T. Gaebel, F. Jelezko, P. Hemmer, and J. Wrachtrup, Spin-flip, and spin-conserving optical transitions of the nitrogen-vacancy centre in diamond, *New J. Phys.* **10**, 045004 (2008).
- [36] N. Aslam, G. Waldherr, P. Neumann, F. Jelezko, and J. Wrachtrup, Photo-induced ionization dynamics of the nitrogen vacancy defect in diamond investigated by single-shot charge state detection, *New J. Phys.* **15**, 013064 (2013).
- [37] N. B. Manson, J. P. Harrison, and M. J. Sellars, Nitrogen-vacancy center in diamond: Model of the electronic structure and associated dynamics, *Phys. Rev. B* **74**, 104303 (2006).
- [38] P. Neumann, J. Beck, M. Steiner, F. Rempp, H. Fedder, P. R. Hemmer, J. Wrachtrup, and F. Jelezko, Single-shot readout of a single nuclear spin, *Science* **329**, 542 (2010).
- [39] D. Pagliero, A. Laraoui, J. Henshaw, and C. A. Meriles, Recursive polarization of nuclear spins in diamond at arbitrary magnetic fields, *Appl. Phys. Lett.* **105**, 242402 (2014).